Paper 26


Proceedings of the Eleventh International Conference
on Computational Structures Technology,
B.H.V. Topping, (Editor),
Civil-Comp Press, Stirlingshire, Scotland

# Numerical Analysis and Model Calibration for Perforated Pallet Rack Uprights

**A. Crisan[1], V. Ungureanu[1,2] and D. Dubina[1,2]**
**[1] Department of Steel Structures and Structural Mechanics**
**Laboratory of Steel Structures**
**"Politehnica" University of Timisoara, Romania**
**[2] Romanian Academy-Timisoara Branch, Romania**

## Abstract

The present paper summarizes the numerical investigation on two perforated pallet rack upright sections in the interactive buckling range using erosion of critical bifurcation load (ECBL) approach. The numerical models were calibrated against the results of an extensive experimental program carried out at the CEMSIG Research Center within Civil Engineering Faculty of "Politehnica" University of Timisoara.

The experimental program was based on the guidelines of the pallet rack systems design code EN15512:2009 and comprises stub column tests, tests on upright sections with the length equal with the distance between two subsequent nodes, tests on upright sections having the critical length corresponding to distortional buckling and tests on uprights having the length (calibrated using the ECBL approach) in the interactive buckling range. Besides the experimental tests on perforated sections, foreseen by EN15512:2009, unperforated sections were tested in order to determine the influence of perforations on sectional capacity and on buckling resistance. Also, within the experimental program were determined the mechanical properties of base material, the mechanical properties of material extracted from cold-formed section, the residual stresses and the geometric imperfections, sectional and overall.

For numerical analysis, the commercial finite element software package ABAQUS was used. The numerical analyses were conducted in order to extend the experimental database and to obtain more information regarding the behaviour of studied sections. Using the calibrated numerical models, a sensitivity analysis was performed in order to identify the critical geometric imperfections based on the maximum erosion of critical load. Further, based on the ECBL approach and using the numerically obtained compression capacity for studied sections, the practical erosion was computed, and based on its design value the $\alpha$ imperfection factor was calibrated. From the point of view of design procedure, the perforations can be treated as geometric imperfections. The presence of perforations increase the value of the $\alpha$ imperfection factor. The numerically results obtained were compared with the experimental tests and the results obtained using design procedure defined in EN15512:2009.

**Keywords:** erosion of critical bifurcation load, erosion coefficient, imperfection factor, rack, upright, finite element method.

# 1 Introduction

Pallet rack uprights systems are usually made of thin-walled cold-formed steel sections that contain arrays of holes along the longitudinal axis of the member. These perforations allows for hook-in end connectors to be used in order to obtain the so called hook-in beam-to-column connections.

Despite their lightness, these structural systems are able to carry very high loads and can also raise considerable height. Usually, upright members are of mono-symmetrical sections, subjected to axial compression and bending about both axes. The complex shape for these sections is determined based on two considerations: ease of assembling and structural efficiency (cost effective).

The design of these structures is based on experimental tests prescribed by specific codes. Organizations like Fédération Européenne de la Manutention, Rack Manufacturers Institute, German Institute for Quality Assurance and Marketing and Storage Equipment Manufacturing Association developed and published norms and design recommendations: [1], [2], [3], [4]. In 2008, in Europe was submitted for approval the pre-norm prEN15512:2008 [5], which in March 2009 was accepted and published in its final form as EN15512:2009 [6].

According to European design code, EN15512 [6], tests on: (1) stub columns, to determine the influence of perforations and local buckling on the ultimate capacity of the cross-sections and, (2) tests on specimens of length equal to the distance between two subsequent nodes of upright members, to check the effects of distortional buckling, are requested only for single sections. Additional, upright frame units are tested in compression, with the force applied on a single branch, in order to observe the global instability behaviour of upright members.

However, depending on the cross-section dimensions, the distance between two subsequent nodes is often larger than distortional critical length and, in such cases the test results correspond rather to the distortional-global interaction, than to pure distortion. For the consistency of testing with the target phenomenon, specimens having the lengths corresponding to pure distortional buckling would be necessary to be tested and after, the distortion characteristic load could be used in the interactive distortional-overall buckling strength analytical evaluation.

To study the problem of buckling mode interaction involving coupling between distortional and overall modes an extensive experimental program would be required in order to determine, experimentally, the erosion of buckling strength for perforated sections in compression, as well the effect of imperfection.

To reduce the number of experimental tests, the European design code [6] allows for the use of numerical approaches that takes rational account the influence of perforations (i.e. finite element analysis), providing that the models are validated by relevant tests.

# 2 Literature review

As mentioned before, the optimized shape of pallet rack structures lead to complex shape for these sections, determined based on two considerations: ease of assembling and structural efficiency (cost effective). In order to raise the buckling strengths of the webs, small groove stiffeners were folded in. This eliminated the local buckling problem, but created what Thomasson [7] called a "local-torsional" problem – i.e. distortional buckling. The research regarding the behaviour of cold-formed steel columns began in the 1940's. Since then, distortional buckling came in and out of the spotlight under different names. Schafer and Hancock [8] present a detailed history of distortional buckling for columns, including the use of numerical methods for the study of different instability problems.

The significant progress from the last two decades in application of numerical techniques for the simulation of complex behaviour of cold-formed steel members, including interactive buckling, enabled for applying the so called numerical testing instead of laboratory tests. Of course, it is still necessary to calibrate the numerical models by a reference test, but after that, those models can be reliable enough to replace the actual experimental tests.

A very important part in numerical analysis of thin walled section is played by linear buckling analysis. It can be used to analyse and approximately predict the buckling behaviour of a member, and, in the same time, modern design procedures for member stability checks are based on the outcome of such analysis. Three methods can be applied to perform linear buckling analyses: the finite strip method (FSM), the generalized beam theory (GBT) and the finite element method (FEM).

Two general reports related to numerical models and methods applied in the simulation, presented in two editions of Coupled Instability in Metal Structures Conferences, CIMS 1996 and 2000, by Rasmussen [10] and Sridharan [11], reviewed the main contributions and milestones in the progress at the date. They concluded the most used computational models are the ones applying the semi-analytical [12] and spline finite strip [13] and the finite element methods [14]. At CIMS 2008, summarizing the advances and developments of computational modelling of cold-formed steel, Schafer [15] emphasized that the primarily focus is the use of semi-analytical finite strip method, considering the implementation of the constrained finite strip method (cFSM) [16]. This method allows for discrete separation of local, distortional and global deformations, and collapse modelling using shell finite elements.

A good alternative to that is the application of modal decomposition via generalised beam theory (GBT), method which achieved a significant development in the last decade by works of the Lisbon team led by Camotim [1], which makes possible to select the deformation modes to be considered in the analysis. At this moment it is possibly to analyse with GBT members made of one or several isotropic or orthotropic materials, with various common support conditions.

Camotim et al. [18] summarise the main concepts and procedures involved in performing a GBT buckling analysis together with the development and numerical implementation of a GBT-based beam finite element formulation, which includes local, distortional and global deformation modes and can handle general loadings.

GBT-based results were compared with values yielded by shell finite element analyses; despite the huge difference between the numbers of degrees of freedom involved in the two analyses (orders of magnitude apart), an excellent agreement was found in all cases.

The problem when both GBT and FSM/cFSM when applied to pallet rack upright sections is that they cannot deal with perforations. These methods can only consider variations at the cross-section level and cannot easily reproduce any discrete variation along the length of the member. However, in view of the advantages that the use of GBT and FSM offer, it is worth trying to expand their application to perforated rack columns. The FEM is the most versatile, since it can be easily adapted to complex geometries and different load and member end conditions. However, its computational cost is high and it is usually implemented in difficult to learn software.

Numerous investigations on the design of perforated cold-formed steel members can be found in the scientific literature. The holes in are usually isolated or far apart from each other and their size is, usually, large. Szabo & Dubina [19] and Moen & Schafer [20] adapted the effective width method and, respectively, the DSM [21] for members with perforations.

Pallet rack columns, on the other hand, present smaller perforations that are uniformly distributed all along their length to facilitate the connection with the other members of the structure. Several investigations on this type of perforated members were conducted in order to develop an analytical design method to reduce the number of experimental testing.

Preliminary calculations on rack columns, applying the direct strength method (DSM), were carried out by Casafont et al. [22].

Conventional procedures for member stability checks based on buckling curves would be much more practical if they could be adapted for members with perforated walls.

Present paper presents the numerical approach for the study of buckling modes interaction (distortional and overall). A numerical imperfection sensitivity study was conducted in order to determine the maximum erosion of critical bifurcation load due to mode coupling, imperfections and perforations. Using the ECBL approach [23] the maximum value of erosion was computed and based on its value, a corresponding imperfection factor.

# 3 Experimental and numerical data

## 3.1 Experimental program

The cross-section shapes of studied sections, both for brut and perforated (i.e. net) sections are shown in Figure 1. Two series have been tested, RS125×3.2 and RS95×2.6, of perforated-to-brut cross-section ratios, $A_N/A_B$, of 0.806 and 0.760, respectively.

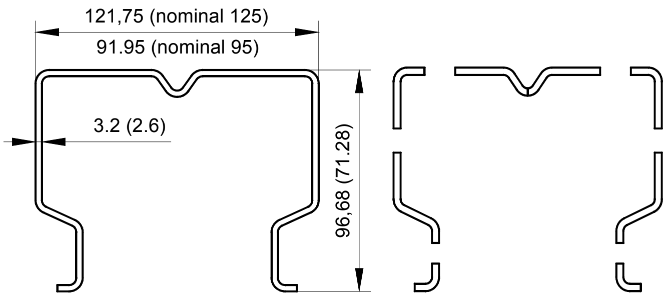


Figure 1: Specimen cross-section – brut (RSB) and perforated (RSN)

Figure 2 presents the perforation details for the studied cross-sections. The pitch is 50mm for both studied sections, RSN125×3.2 and RSN95×2.6 respectively.

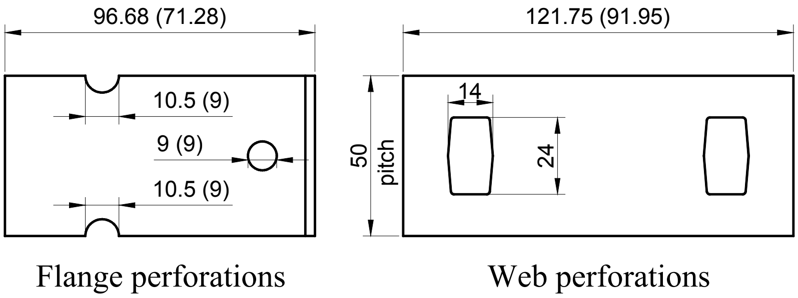


Figure 2: Perforation details

The experimental program, based on the specifications of European design code [6] comprises four types of compression tests, as follows: (1) Stub columns (s); (2) Upright member specimens for distortional buckling (u); (3) Specimens of lengths equal with the half-wave length of distortional buckling (d); (4) Specimens of lengths corresponding to interactive buckling range (c).

The test setup was approximately the same for all tested specimens. The compression load was transmitted to the base plates via 30 mm thick pressure pads (to avoid the undesired deformations of the pads during the test). The pressure pads were prepared with a 5 mm indentation in order to receive a 40 mm diameter steel ball bearing. The test setup for stub column test is presented in detail in Figure 3 (*a* is base/cap plate, *b* is buckling length of the specimen and *c* is the length of the cold-formed stub upright).

The ball bearing was positioned on the symmetry axis of the cross section in between the position of gross and the minimum cross section centres of gravity.

The theoretical position of the ball bearing was on the same line with gravity centres at the both ends, in order to avoid any accidental loads. For obtaining a static load, the specimens were loaded in displacement control at a steady rate of 0.2 mm/minute.

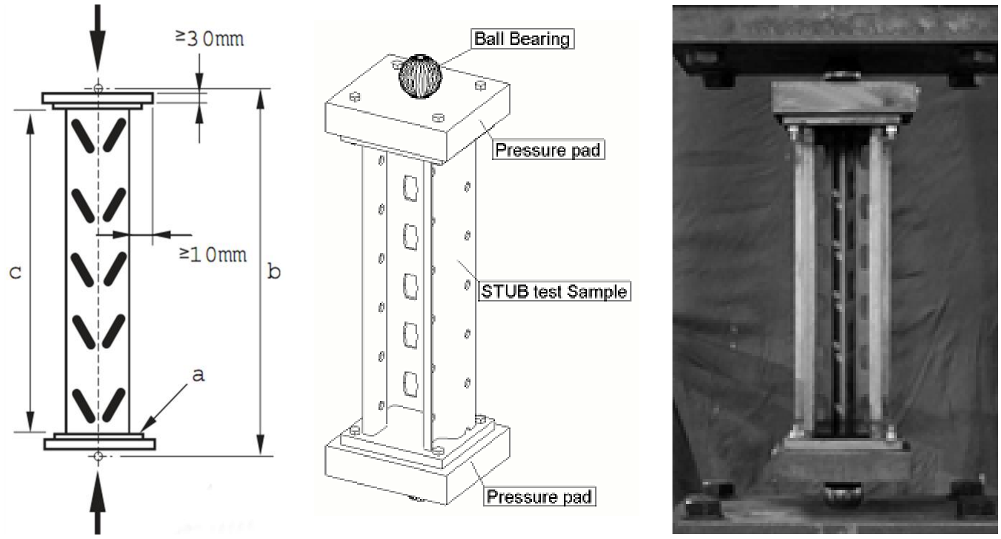


Figure 3: Stub column test setup

Additional restraints were foreseen for specimens of lengths corresponding to interactive buckling range (c) in order to restrain the torsion.

The experimental program was explicitly presented by the authors in [24], [25].

## 3.2 Numerical model calibration and validation

The numerical models applied to simulate the behaviour of studied sections, have been created using the commercial FE program, ABAQUS/CAE [26]. The numerical models were calibrated to replicate the physical tests. Different element types and mesh sizes were tested in order to find a structured mesh able to assimilate the perforations, to find the optimum number of elements from the point of view of ultimate force accuracy and, in the same time, to reduce the computational time. Rectangular 4-noded shell elements with reduced integration (S4R) were used to model the thin-walled cold-formed members.

In order to create a reliable mesh and to account the holes present along the specimen's length a mesh size of about 5×5mm was chosen (see Figure 4). The elements were constrained to a rectangular form and a structured mesh was used.

The base plates and pressure pads were modelled using RIGID BODY with PINNED nodes constraints. The reference point for the constraints was considered the centre of the ball bearings (55mm outside the profile), in the gravity centre of the cross-section (see Figure 5). For numerical simulations, the specimens were considered pinned at one end and simply supported at the other one. For the pinned end, all three translations together with the rotation along the longitudinal axis of the profile were restrained, while the rotations about maximum and minimum inertia axes were allowed. For the simply supported end, the translations along section axis and the rotation about longitudinal profiles axis were restrained, while the rotations about major and minor inertia axis together with longitudinal translation were allowed.

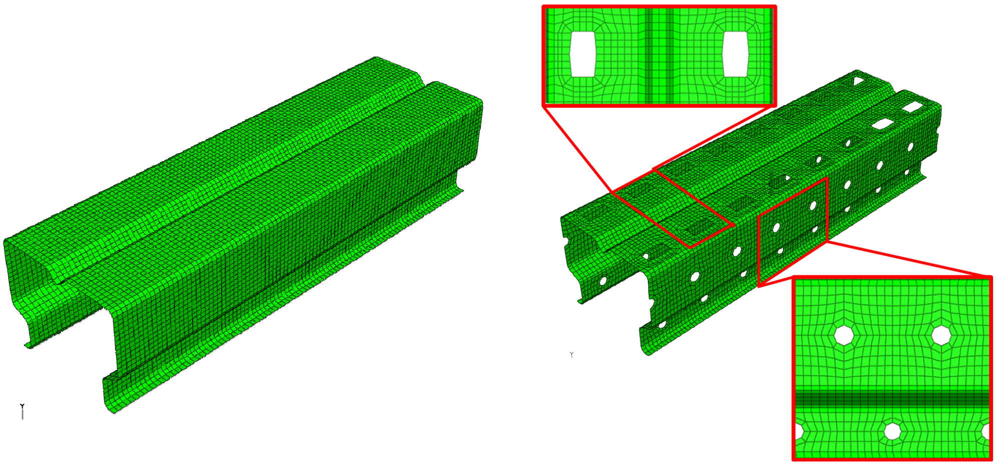

section without perforations section with perforations

Figure 4: Mesh details for RS125 STUB specimen (unde este referita?)

The pinned end was considered to replicate the end support of the real tested specimen, while the simply supported end was considered to reproduce the loading machine end, allowing for direct force/displacement specification. For test specimens, the rotation about longitudinal axis was prevented by friction, while for numerical model the rotation was restrained, in order to remove rigid body displacements (rotations along the longitudinal axis, in this case).

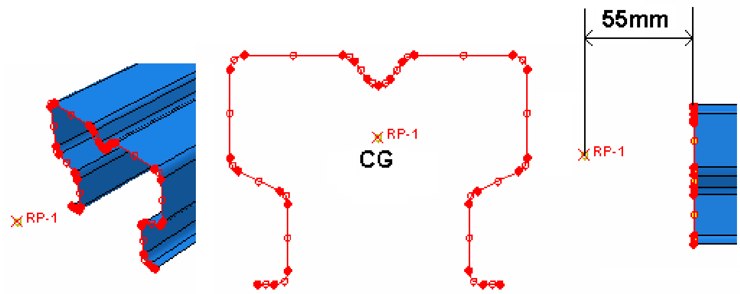


Figure 5: FE model end constraints

The analysis was conducted into two steps. The first step consists into an eigen buckling analysis (LBA), in order to find a buckling mode or combination of buckling modes, affine with the relevant measured imperfections. After imposing the initial geometric imperfection, obtained as a linear combination of eigen buckling modes from the previous step, a GMNIA analysis with arc-length (static, Riks) solver was used to determine the profiles capacity. A unit displacement was applied at the simply supported end, incremented during the analysis, in order to simulate a displacement controlled experimental test.

Different element types and material behaviours were analysed from the point of view of ultimate force and failure mode. In Table 1 are presented the failure loads obtained numerically for the considered element types. For these analyses, the material behaviour i.e. yielding stress distribution across the section and the Young's modulus value were those experimentally obtained.

| Element type | S4 | S4R | S8R5 | S8R |
|---|---|---|---|---|
| Ultimate load [kN] | 463.06 | 461.70 | 463.02 | 463.01 |
| Analysis time[1] | 0:01:40 | 0:01:38 | 0:05:29 | 0:04:04 |
| Analysis time[2] | 0:05:46 | 0:04:00 | 0:27:04 | 0:19:14 |
| Total time | 0:07:26 | 0:05:38 | 0:32:33 | 0:23:18 |

[1]buckling analysis time and [2]static Riks analysis time.

Table 1. Ultimate load and analysis time per element type

It can be observed that for this specific type of analysis and section, the influence of element type is insignificant. It can be noted that the numerical model behaviour is no influenced by the element type. Based on these observations, the S4R finite element type was chosen for further analyses. S4R is a robust, general-purpose element that is suitable for a wide range of applications. It is a 4-noded doubly curved quadrilateral, stress/displacement shell element with reduced integration and a large-strain formulation that have 6 DOFs per node.

A parametric study regarding the material properties i.e. Young's modulus and real yield stress distribution was done. In Table 2 are presented the considerate cases together with the numerically obtained ultimate forces. The effect of residual stresses was considered. The residual stresses were modelled as initial stress state. The method used to describe the initial stress state allows for direct specification of stress value for each individual integration point.

| Case no. | Young's Modulus [N/mm$^2$] | $f_y$ [N/mm2] | Residual stresses | Geometric imperfection | Load ecc. | Ultimate force |
|---|---|---|---|---|---|---|
| 1 | 202941 | exp[1] | yes | yes | yes | 448.634 |
| 2 | 202941 | exp[1] | Yes | yes | no | 460.936 |
| 3 | 202941 | exp[1] | Yes | no | yes | 526.804 |
| 4 | 202941 | exp[1] | no | no | yes | 531.583 |
| 5 | 202941 | exp[1] | no | no | no | 541.873 |
| 6 | 202941 | exp[1] | no | yes | yes | 461.701 |
| 7 | 202941 | $f_{ya}$[2] | yes | yes | yes | 442.382 |
| **8** | **202941** | **$f_{ya}$[2]** | **no** | **yes** | **yes** | **455.163** |
| 9 | 210000 | $f_{ya}$[2] | yes | yes | yes | 444.352 |
| 10 | 210000 | $f_{ya}$[2] | no | yes | yes | 457.51 |
| 11 | 202941 | $f_{yb}$[3] | yes | yes | yes | 415.026 |
| 12 | 202941 | $f_{yb}$[3] | no | yes | yes | 426.854 |
| 13 | 210000 | $f_{yb}$[3] | yes | yes | yes | 417.092 |
| 14 | 210000 | $f_{yb}$[3] | no | yes | yes | 428.657 |
| exp | - | - | - | - | - | 453.90 |

[1]experimentally obtained yield stress distribution;
[2]average yield stress, $f_{ya}$, obtained in accordance with EN1993-1-3 [27];
[3]yield stress of base material, $f_{yb}$.

Table 2. Cases considered for parametric analysis

It can be observed that the influence of residual stress is small (less than 3%). Since the effects of residual stresses are not the primary objective of the present study, for further analysis, their effects will be ignored, unless otherwise specified. Even more, when the material properties of the cross-section are established from coupons cut from within the section, the effect of flexural residual stresses is inherently present, and no need to be explicitly defined in the finite element model [30].

It must be mentioned that for all considered numerical models, the failure modes were in accordance with the failure mode observed on reference experimental test.

The calibrated numerical model was validated against experimental tests for all tested profiles sets. Table 3 presents the values of ultimate load from numerical simulations and the experimental ones for all types of members (stub, distortional, upright and in the coupling range), for both RS125×3.2 and RS95×2.6 cross-sections, with and without perforations.

| RSBs125×3.2 | | RSNs125×3.2 | | RSBs95×2.6 | | RSNs95×2.6 | |
|---|---|---|---|---|---|---|---|
| EXP | FEM | EXP | FEM | EXP | FEM | EXP | FEM |
| 487.05 | 486.13 | 411.02 | 422.98 | 338.88 | 335.15 | 274.33 | 272.01 |
| RSBd125×3.2 | | RSNd125×3.2 | | RSBd95×2.6 | | RSNd95×2.6 | |
| EXP | FEM | EXP | FEM | EXP | FEM | EXP | FEM |
| 440.79 | 440.78 | 394.62 | 397.04 | 325.10 | 331.05 | 262.67 | 255.47 |
| RSBu125×3.2 | | RSNu125×3.2 | | RSBu95×2.6 | | RSNu95×2.6 | |
| EXP | FEM | EXP | FEM | EXP | FEM | EXP | FEM |
| 386.72 | 384.40 | 347.26 | 344.00 | 279.65 | 285.96 | 223.33 | 231.89 |
| RSBc125×3.2 | | RSBc125×3.2 | | RSBc95×2.6 | | RSBc95×2.6 | |
| EXP | FEM | EXP | FEM | EXP | FEM | EXP | FEM |
| 317.89 | 316.67 | 293.62 | 292.9 | 220.29 | 220.26 | 168.88 | 177.11 |
| (s) Stub columns; (d) Specimens of lengths equal with the half-wave length of distortional buckling; (u) Upright member specimens; (c) Specimens of lengths corresponding to interactive buckling range. N/B – perforated/brut | | | | | | | |

Table 3. Ultimate load [kN] – Experimental vs. FEM

As it can be observed in Table 2, the model using the experimentally determined properties of base material ($E$=202941N/mm$^2$), a bilinear material behaviour with $f_y$ determined , obtained in accordance with EN1993-1-3 [27] and no residual stresses is in accordance with the experimental test. Since the numerical results, obtained using this numerical model (Table 2, case 8), are in good agreement with experimental test results, it will be further used for all numerical analyses.

Furthermore, in Figure 6 are presented the characteristic failure modes for experimentally tested and numerically simulated specimens. Obviously, in all the cases a good agreement exists between the results of FE analyses and experimental ones.

The decomposition method used in this case is limited to symmetric sectional buckling and/or global buckling. Further development and more complex measuring are required in order to replicate all experimentally obtained failure modes.

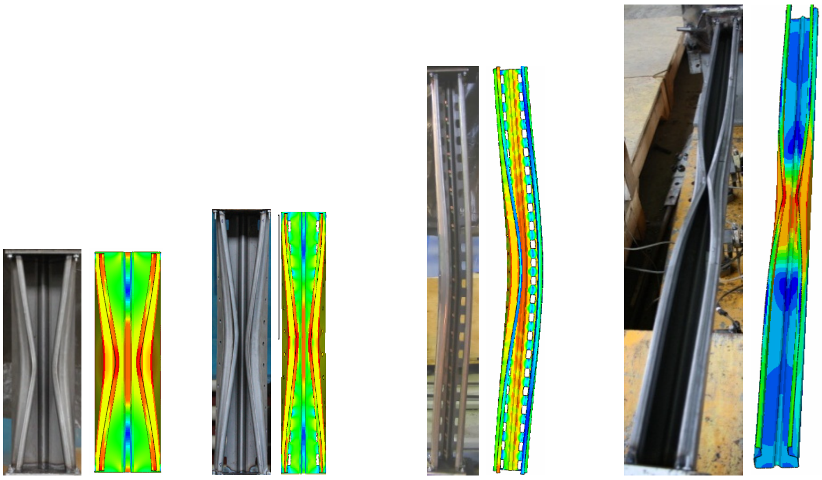

RSBs 125×3.2 RSNd 125×3.2 RSNu 95×2.6 RSBc95×2.6

Figure 6: Failure modes – Experimental vs. FE models

Based on the results obtained from numerical simulations, it can be noted that from the point of view of maximum load, the numerical model is able to accurately replicate the experimental tests. For specimens with increased length, where global and sectional imperfections are of same importance, a more complex imperfections measurement is recommended. The measurements should allow the decomposition of geometric imperfections into sectional and global components that can afterwards be used to reconstruct the initial deformed shape.

# 4 Imperfection sensitivity analysis

## 4.1 Determination of coupling point according to ECBL

The interactive buckling approach based on ECBL method is largely presented in [23]. The principle of this method is summarized here only. Assuming the two theoretical simple instability modes that couple, in a thin-walled compression member, are the Euler bar instability mode, $\overline{N}_E = 1/\overline{\lambda}^2$ ($\overline{\lambda}$= relative member slenderness) and the distortional instability mode described by means of the reducing factor of area $\overline{N}_D$. The resulting eroded curve for coupled instability mode is $\overline{N}(\overline{\lambda}, Q_D, \psi)$ (see Figure 7).

Critical load maximum erosion (due both to the imperfections and coupling effect) occurs in the instability mode interaction point, M ($\overline{\lambda} = 1/Q_D^{0.5}$) where, the erosion coefficient $\psi$ is defined as:

$$\psi = \overline{N}_D - \overline{N} \tag{3}$$

in which $\overline{N}(\overline{\lambda}, \overline{N}_D, \psi)$ is the relative interactive buckling load and $\overline{N}_D = N_{cr,D}/f_y \cdot A$; $A$ = is the cross-section area; $N_D$ = is the ultimate capacity corresponding to distortional buckling; $\overline{N} = N/N_{pl}$ is the relative axial load; $N$ = is the axial load; $N_{pl} = f_y \cdot A$ is the full plastic resistance of the member; $\overline{\lambda}$ = is relative slenderness of compression member.

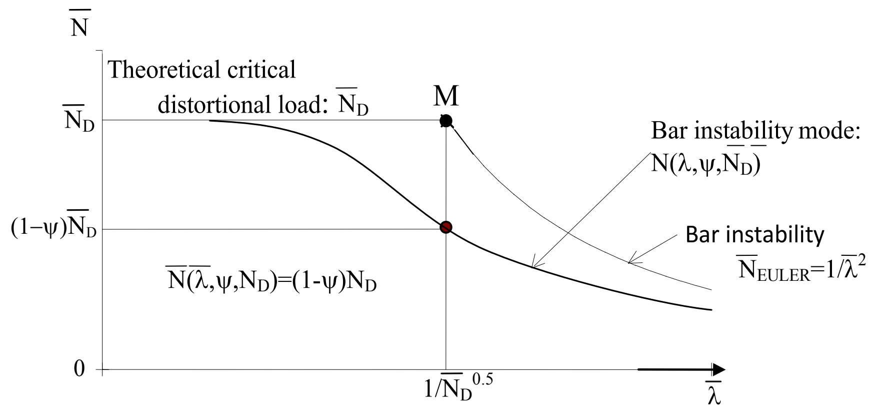


Figure 7: The interactive buckling model based on the ECBL theory

If $\overline{\lambda} = 1/\overline{N_D}^{0.5}$ is introduced, it results an imperfection factor corresponding to the distortional-global buckling:

$$\alpha = \frac{\psi^2}{1-\psi} \cdot \frac{\sqrt{\overline{N_D}}}{1-0.2\sqrt{\overline{N_D}}} \tag{4}$$

Equation 4 represents the new formula of $\alpha$ imperfection factor which should be introduced in European buckling curves in order to adapt these curves to distortional-overall interactive buckling.

The coupling point between distortional (D) and global (F) buckling modes is determined following the ECBL approach as shown in Figure 7. On this purpose, FE analyses were performed to simulate the influence of different types of imperfections in the coupling point. Because the interest is to observe the erosion of critical bifurcation load, this time, the ECBL approach is applied considering the distortional critical load, obtained for the relevant section by an eigen buckling analysis, in interaction with Euler buckling of the corresponding bar member.

Table 4 shows the reference values for critical and ultimate sectional loads obtained numerically and experimentally for the studied sections.

Linear Buckling Analysis (LBA) using ABAQUS was used to determine the relevant sectional failure mode to be considered when determining the sectional capacity (e.g. local or distortional buckling, squash load) for studied cross-sections.

Table 5 presents the lengths corresponding to the theoretical interactive buckling loads (e.g. in the point of $\overline{\lambda} = \sqrt{1/\overline{N_D}}$, $\overline{N_D} = \overline{N}_{cr,D}$) determined via the ECBL approach, in the interactive buckling point, M, for each section.

| Section | RSN125×3.2 | RSN95×2.6 |
|---|---|---|
| Length [mm] | 600 | 500 |
| Distortional buckling load* ($N_{cr,D}$) [kN] | 370.48 | 340.78 |
| Distortional ultimate load** ($N_{D,u}$) [kN] | 388.35 | --- |
| Stub ultimate load*** ($N_{S,u}$) [kN] | 407.79 | 279.27 |
| Squash load**** ($N_{pl}$) [kN] | 480.94 | 286.72 |
| * distortional buckling load determined using LBA; ** experimental failure load corresponding to "distortional" specimens – mean values; *** experimental failure load corresponding cu stub column specimens – mean values; **** $N_{pl}=A \cdot f_y$ | | |

Table 4. Sectional capacity and distortional buckling load

| Profile | $N_{cr,D}$ [kN] | $N_{pl}$ [kN] | $\overline{N}_D$ | Coupling length [mm] |
|---|---|---|---|---|
| RSN125 | 370.48 | 480.94 | 0.770 | 2559 |
| RSN95 | 340.78 | 286.72 | 1.000 | 1667 |
| RSKB90 | - | 303.6 | 1.000 | 1460 |
| RSKN90 | - | 343.2 | 1.000 | 1550 |

Table 5. Lengths corresponding to the theoretical interactive buckling

For the case of RSK90×2.4 sections, in accordance with the LBA analysis conducted, no local minimum was determined (no local, nor distortional).

It can be observed, once again, that for RS95N cross-sections, the critical load corresponding to distortional buckling is greater than the cross-section squash load. In this case the $\overline{N}_D$ value has to be limited to 1.00. Based on this limitation, it can be said that for RS95 section, with and without perforation, there is no classical interactive buckling. However, since the section fails in such a case by a local plastic mechanism we could speak about a plastic – elastic buckling interaction. In order to compute the interactive buckling length for perforated sections, the gross section properties have been used.

## 4.2 Geometric imperfections

In this chapter the study focuses on the sensitivity to imperfections of pallet rack sections in compression, having the member length equal to the interactive buckling length, which was established according to ECBL procedure. Figure 8 shows the geometrical imperfections, considered in the analysis, e.g. distortional (d ±), flexural about the minor axis (f ±), and coupling of these two (f ± d ±). Also, load eccentricities, located on the axis of symmetry, were taken into consideration.

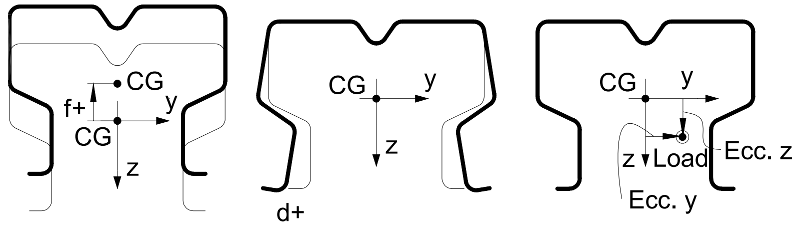

Figure 8: Example of considered simple imperfections (f and d)

In case of flexural-torsional buckling (FT), both initial deflection and initial twisting imperfection (ft) were considered together, according to Australian Standard AS4100 [31]. The code recommendations for the initial deflection, ($f_0$), and for initial twist, ($\phi_0$) are given by Equations 5 and 6:

$$1000 f_0 / L = 1000\phi_0 \left(M_{cr} / N_{cr} L\right) = -1 \quad \text{for} \quad \lambda_{LT} \geq 0.6 \tag{5}$$

$$1000 f_0 / L = 1000\phi_0 \left(M_{cr} / N_{cr} L\right) = -0.001 \quad \text{for} \quad \lambda_{LT} < 0.6 \tag{6}$$

where: $N_{cr}$ = is column elastic critical buckling (Euler) load about minor axis; $M_{cr}$ = is elastic critical moment for lateral-torsional buckling; $\lambda_{LT}$= is the lateral-torsional slenderness; $L$ = is length of the member.

Due to the fact that the global flexural buckling mode about the minor axis has the minimum value for the studied sections the global imperfection considered for coupling was considered a global bow imperfection.

Figure 9 presents an example where coupled imperfections, distortional and flexural, were applied in the numerical model for a perforated section, together with the corresponding failure modes, numerically simulated and experimentally tested specimens.

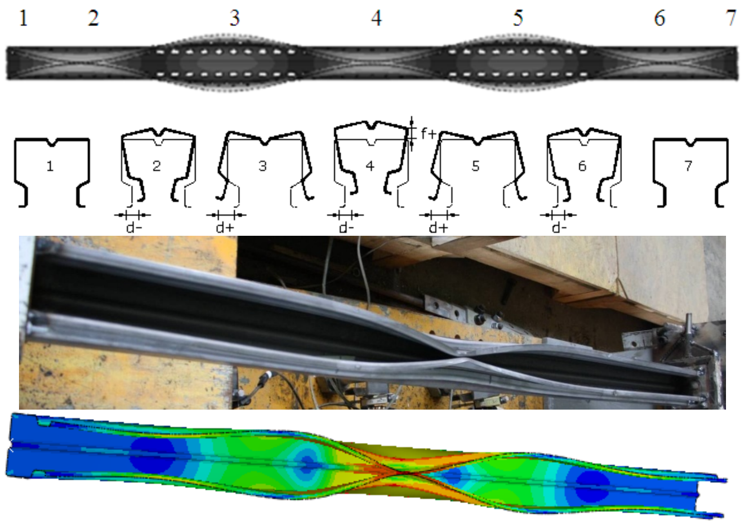

Figure 9: Coupled imperfections (*f*+ and *d*+) considered in numerical analysis; numerical vs. experimental failure modes

## 4.3 Imperfection sensitivity study

On this purpose, the most influential imperfections have to be identified. According to the ECBL approach [23], the main goal is to observe the erosion of practical critical load. Consequently, an imperfection sensitivity study was conducted in order to identify the most critical imperfection or imperfection combination.

As observed in Table 5 for RS95×2.6 section there is no classical buckling mode interaction. Further, the present imperfection study will be focused on RS125 section and it is a continuation of the study presented by the authors in [24] and [32].

Due to the fact that in practice, pallet rack upright sections are more sensitive to flexural-torsional buckling than flexural buckling, another section was considered for the sensitivity study. The section is presented in Figure 10. Koen [33] presented a series of experimental tests results and numerical analyses for this section.

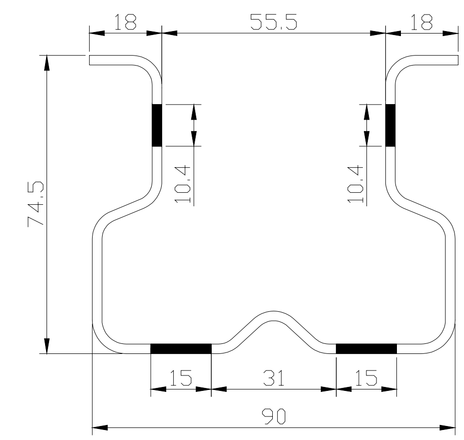


Figure 10: Geometric dimensions for pallet rack upright section [33]

The section will be further referred to as RSKB90×2.4 for the section without perforations and RSKN90×2.4 for the section with perforations.

The imperfections used for this study are: distortional symmetric imperfection (ds), distortional asymmetric imperfection (da) (only for RSN125×3.2 section), flexural bow imperfection about the minor inertia axis (f), loading eccentricities on both axes (independent and coupled – EY, EZ, EY-EZ) and flexural-torsional imperfection (FT). The distortional imperfection, symmetric and asymmetric, was scaled to 0.5*t*, 1.0*t* and 1.5*t*, the flexural bow imperfection was scaled to *L*/750, *L*/1000 and *L*/1500, while the flexural-torsional imperfection was considered in accordance with the provisions of Australian design code [31]. The loading eccentricities were varied on both sectional axes (±6mm), independently and together, as an oblique eccentricity.

In Table 6 are presented the considered simple imperfections, sectional, global and loading eccentricities for RSN125×3.2 section.

| Imperfection | RSN125×3.2 | | RSKB90×2.4 | | RSKN90×2.4 | |
|---|---|---|---|---|---|---|
| | $\psi$ | $\alpha$ | $\psi$ | $\alpha$ | $\psi$ | $\alpha$ |
| ds – 0.5 $t$ | 0.236 | 0.078 | 0.168 | 0.043 | 0.279 | 0.135 |
| ds – 1.0 $t$ | 0.339 | 0.185 | 0.235 | 0.090 | 0.313 | 0.179 |
| ds – 1.5 $t$ | 0.398 | 0.280 | 0.290 | 0.148 | 0.386 | 0.303 |
| da – 0.5 $t$ | 0.152 | 0.029 | 0.154 | 0.035 | 0.298 | 0.158 |
| da – 1.0 $t$ | 0.245 | 0.085 | 0.219 | 0.077 | 0.346 | 0.228 |
| da – 1.5 $t$ | 0.321 | 0.162 | 0.271 | 0.126 | 0.404 | 0.341 |
| f – $L$/750 | 0.240 | 0.081 | 0.196 | 0.060 | 0.283 | 0.140 |
| f – $L$/1000 | 0.216 | 0.063 | 0.231 | 0.087 | 0.305 | 0.168 |
| f – $L$/1500 | 0.181 | 0.043 | 0.264 | 0.118 | 0.335 | 0.211 |
| FT | 0.240 | 0.081 | 0.302 | 0.163 | 0.410 | 0.356 |
| EY 2 | 0.169 | 0.037 | 0.248 | 0.102 | 0.380 | 0.291 |
| EY 4 | 0.196 | 0.051 | 0.324 | 0.194 | 0.428 | 0.400 |
| EY 6 | 0.224 | 0.069 | 0.378 | 0.287 | 0.466 | 0.508 |
| EZ -6 | 0.313 | 0.152 | 0.383 | 0.297 | 0.470 | 0.520 |
| EZ -4 | 0.272 | 0.108 | 0.327 | 0.198 | 0.427 | 0.397 |
| EZ -2 | 0.210 | 0.059 | 0.241 | 0.096 | 0.370 | 0.272 |
| EZ 2 | 0.216 | 0.063 | 0.285 | 0.142 | 0.349 | 0.234 |
| EZ 4 | 0.255 | 0.093 | 0.378 | 0.288 | 0.433 | 0.414 |
| EZ 6 | 0.285 | 0.121 | 0.441 | 0.435 | 0.492 | 0.595 |
| EY-EZ 0 | 0.157 | 0.031 | 0.069 | 0.006 | 0.276 | 0.132 |
| EY-EZ 6 | 0.321 | 0.162 | 0.459 | 0.487 | 0.523 | 0.718 |
| EY-EZ 4 | 0.276 | 0.112 | 0.400 | 0.332 | 0.474 | 0.535 |
| EY-EZ 2 | 0.215 | 0.063 | 0.308 | 0.171 | 0.409 | 0.353 |
| EY-EZ -2 | 0.223 | 0.068 | 0.308 | 0.172 | 0.398 | 0.328 |
| EY-EZ -4 | 0.270 | 0.106 | 0.403 | 0.340 | 0.471 | 0.523 |
| EY-EZ -6 | 0.307 | 0.145 | 0.467 | 0.511 | 0.522 | 0.711 |

Table 6. $\psi$ erosion coefficient and $\alpha$ imperfection factors for simple imperfections

In Table 6 can be easily observed that for the RSK90×2.4 section, even if there is no real buckling mode interaction, the presence of perforations affects the values of corresponding erosions, and consequently, the values of the imperfection factors. In the same time, it can be observed that for RSK90×2.4 sections, the value corresponding to FT imperfection is higher than those corresponding to flexural imperfections. This can be explained by the fact that, as mentioned before, the section is more sensitive to flexural-torsional buckling

Table 7 presents the coupled imperfections considered for the RSN125×3.2 section.

It is easy to observe that the combination (f – $L$/750, ds – 1.5 $t$) of imperfections is the most critical one. However, statistically is not recommended to combine all imperfections to cumulate their negative effects, because their random compensation.

| Imperfection | $\psi$ | $\alpha$ |
|---|---|---|
| f – $L$/750, ds – 0.5$t$ | | |
| EY 2 | 0.339 | 0.185 |
| EY 4 | 0.342 | 0.189 |
| EY 6 | 0.346 | 0.195 |
| EZ 6 | 0.425 | 0.334 |
| EZ 4 | 0.404 | 0.292 |
| EZ 2 | 0.376 | 0.241 |
| EZ -2 | 0.279 | 0.115 |
| EZ -4 | 0.194 | 0.050 |
| EZ -6 | 0.240 | 0.081 |
| EY-EZ 0 | 0.240 | 0.081 |
| EY-EZ 6 | 0.430 | 0.345 |
| EY-EZ 4 | 0.406 | 0.295 |
| EY-EZ 2 | 0.377 | 0.243 |
| EY-EZ -2 | 0.280 | 0.116 |
| EY-EZ -4 | 0.218 | 0.065 |
| EY-EZ -6 | 0.271 | 0.107 |
| EY 2 | 0.302 | 0.139 |
| EY 4 | 0.305 | 0.142 |
| EY 6 | 0.310 | 0.148 |
| EZ 6 | 0.411 | 0.305 |
| EZ 4 | 0.384 | 0.255 |
| EZ 2 | 0.350 | 0.201 |
| EZ -2 | 0.174 | 0.039 |
| EZ -4 | 0.228 | 0.072 |
| EZ -6 | 0.264 | 0.101 |
| EY-EZ 0 | 0.301 | 0.138 |
| EY-EZ 6 | 0.414 | 0.311 |
| EY-EZ 4 | 0.386 | 0.258 |
| EY-EZ 2 | 0.351 | 0.202 |
| EY-EZ -2 | 0.182 | 0.043 |
| EY-EZ -4 | 0.247 | 0.086 |
| EY-EZ -6 | 0.289 | 0.125 |

| Imperfection | $\psi$ | $\alpha$ |
|---|---|---|
| f – $L$/750, ds – 1.5$t$ | | |
| EY 2 | 0.440 | 0.368 |
| EY 4 | 0.442 | 0.373 |
| EY 6 | 0.443 | 0.375 |
| EZ 6 | 0.493 | 0.510 |
| EZ 4 | 0.479 | 0.469 |
| EZ 2 | 0.461 | 0.420 |
| EZ -2 | 0.413 | 0.309 |
| EZ -4 | 0.374 | 0.238 |
| EZ -6 | 0.276 | 0.112 |
| EY-EZ 0 | 0.440 | 0.368 |
| EY-EZ 6 | 0.495 | 0.517 |
| EY-EZ 4 | 0.480 | 0.472 |
| EY-EZ 2 | 0.462 | 0.422 |
| EY-EZ -2 | 0.413 | 0.309 |
| EY-EZ -4 | 0.376 | 0.241 |
| EY-EZ -6 | 0.298 | 0.135 |
| EY 2 | 0.422 | 0.328 |
| EY 4 | 0.423 | 0.330 |
| EY 6 | 0.425 | 0.334 |
| EZ 6 | 0.483 | 0.480 |
| EZ 4 | 0.467 | 0.436 |
| EZ 2 | 0.447 | 0.385 |
| EZ -2 | 0.387 | 0.260 |
| EZ -4 | 0.326 | 0.168 |
| EZ -6 | 0.261 | 0.098 |
| EY-EZ 0 | 0.421 | 0.326 |
| EY-EZ 6 | 0.485 | 0.486 |
| EY-EZ 4 | 0.467 | 0.436 |
| EY-EZ 2 | 0.447 | 0.385 |
| EY-EZ -2 | 0.387 | 0.260 |
| EY-EZ -4 | 0.330 | 0.173 |
| EY-EZ -6 | 0.285 | 0.121 |

Table 7a. $\psi$ erosion factors and α imperfection factors for coupled imperfections

In terms of $\psi$ interaction factor, Gioncu [34] defined 4 classes of interaction, ranging from WI (weak interaction) with $\psi < 0.1$ to VSI (very strong interaction) for $\psi > 0.5$.

A precise framing for coupled instabilities is very important in order to choose a suitable design strategy. For weak and moderate interaction class, simple design methods based on safety coefficients can be used. In case of strong and very strong interaction, special design methods must be developed.

It can be observed that for the case of RSN125 pallet rack section, the computed erosion can classify the section into medium up to very strong interaction, depending on the considered imperfection.

A sensitivity analysis, considering appropriate value for imperfections, sectional (local or distortional) and global (flexural, torsional or flexural-torsional) should be performed in order to determine the erosion coefficient and, based on its value the, imperfection coefficient.

# 4 Concluding remarks

Both test and numerical simulations have proven the negative influence of interaction between distortional and overall buckling in the case of this particular type of rack sections. The interaction of buckling modes reduces significantly the capacity of perforated members in compression.

In order to reduce the number of experimental testing, a rational sensitivity analysis done using calibrated and validated numerical models can be used in order to determine the imperfections to be considered for the numerical model, when determining the erosion factor.

The ECBL approach can be successfully applied, with a limited number of tests for material properties and stub column tests, using numerical simulations. Considering the maximum values for imperfection recommended in literature, it can be observed that real sections tend to have a higher capacity than the one obtained via numerical simulations. Two main reasons can be identified for this: (1) the real imperfections are lower than those recommended by codes and literature and (2) in real cases, the imperfections randomness partially compensates each other, while in numerical simulation they are cumulatively applied.

The ECBL approach [23] is an excellent procedure that permits the evaluation of erosion of critical bifurcation load as result of interactive buckling. It applies for the interaction of sectional (local or distortional buckling) with global (flexural or flexural-torsional) instabilities.

A design procedure based on EN1993-1-1 [35], coupled with the ECBL approach, applied to calibrate the value of $\alpha$ imperfection factor, can be used to determine the buckling strength of compressed pallet rack uprights. This approach can be used for the case of sectional capacity, defined by local or distortional buckling, or squash load, coupled with overall buckling (i.e. flexural, torsional or flexural-torsional).

A rational sensitivity analysis, supported by reference test, is of paramount importance in order to determine the imperfections to be considered for the numerical model, when determining the erosion factor.

Considering the results presented in previous chapter, it can be said that a correctly calibrated numerical model can be used to perform a sensitivity study, no matter for the buckling modes that couples i.e. distortional and overall flexural buckling in case of RSN125×3.2 section, plastic strength and flexural overall buckling in case of RSN95×2.4 section and plastic strength and flexural-torsional buckling, in case of RSK90×2.4 section.

Moreover, using a correctly calibrated numerical model to perform a sensitivity analysis, on the ECBL approach the maximum erosion and corresponding imperfection factor can be determined for a given section, with or without perforations.

## References


[1] FEM10.2.02:2000, Section X, The design of steel static pallet racking, Revision 1.01, 2000.

[2] RMI:1997, Specification for the design, testing and utilization of industrial steel storage racks, Rack Manufacturers Institute, SUA, 1997.

[3] RAL-RG 614:1990, Storage and associated equipment - Quality assurance, German Institute for Quality Assurance and Marking, Germany, 1990.

[4] AS4084, Australian standard, Steel storage racking, Standards Australia, Homebush, NSW 2140, Australia, 1993.

[5] prEN15512, Steel static storage systems, Adjustable pallet racking systems, Principles for structural design, Published by European Committee for Standardization, Brussels, 2008.

[6] EN15512:2009: Steel static storage systems - Adjustable pallet racking systems - Principles for structural design, CEN, Brussels, 2009.

[7] Thomasson P. Thin-walled C-shaped panels in axial compression. Swedish Council for Building Research. D1:1978, Stockholm, Sweden, 1978.

[8] Schafer B, Hancock G. A History of Distortional Buckling of Cold-Formed Steel Columns,

[9] Moen CD, Schafer BW. Direct strength design of cold-formed steel members with perforations. Research Report RP09-1, The Johns Hopkins University, USA, 2009.

[10] Rasmussen KJR. Numerical simulations and computational models in coupled instabilities, Proceedings of the Second International Conference on Coupled Instabilities in Metal Structures, CIMS'96, 45 - 60, 1996.

[11] Sridharan S. Numerical simulation and computational models for coupled instabilities, Proceedings of the Third International Conference on Coupled Instabilities in Metal Structures, CIMS'2000, 61 - 72, 2000.

[12] Cheung YK. Finite strip method in structural analysis, Pergamon Press, New York, 1976.

[13] Cheung YK, Fan SC. Static analysis of right box girder bridges by spline finite strip method, Proceedings of Institution of Civil Engineering, 75(2), 311-23, 1983.

[14] Bathe K-J. Finite element procedures in engineering analysis, Printice-Hall, Englewood Cliffs, NJ, 1982.

[15] Schafer BW. Computational modelling of cold-formed steel, Proceedings of the Fifth International Conference on Coupled Instabilities in Metal Structures, CIMS'2008, 53 - 60, 2008.

[16] Adany S, Schafer BW. A full modal decomposition of thin-walled, single-branched open cross-section members via constrained finite strip method, Journal of Constructional Steel Research, 64(1), 12-29, 2008.

[17] Bebiano R, Pina P, Silvestre N, Camotim D. GBTUL – Buckling and vibration analysis of thin-walled members, DECivil/IST, Technical University of Lisbon, http://www.civil.ist.utl.pt/gbt, 2008.
[18] Camotim D, Basaglia C, Silvestre N. GBT buckling analysis of thin-walled steel frames: A state-of-the-art report. Thin Walled Structures, 48(10-11), 726–743, 2010.
[19] Szabo IF, Dubina D. Recent research advances on the ECBL approach. Part II: interactive buckling of perforated sections, Thin-Walled Structures, 42, 195-210, 2004.
[20] Moen CD, Schafer BW. Direct strength design of cold-formed steel members with perforations, Research Report, Johns Hopkins University, 2008.
[21] Schafer BW. Review: The Direct Strength Method of cold-formed steel member design. Journal of Constructional Steel Research, 64(7-8), 766-778, 2008.
[22] Casafont M, Caparrós F, Pastor M, Roure F, Bonada J. Linear buckling analysis of perforated steel storage rack columns with the finite strip method. Proceedings of The 6th International Conference on Thin Walled Structures, Timisoara, Romania, Vol. 2, 787 – 794, 2011.
[23] Dubina D. The ECBL approach for interactive buckling of thin-walled steel members, Steel & Composite Structures, 1(1), 75-96, 2001.
[24] Crisan A. Buckling strength of cold formed steel sections applied in pallet rack Structures, PhD thesis, "POLITEHNICA" University of Timisoara, Civil Engineering Faculty, Ed. Politehnica, Seria 5: Inginerie Civila, no. 76, 2011.
[25] Crisan A, Ungureanu V, Dubina D. Behaviour of thin-walled cold-formed steel perforated sections in compression. Part 1 – Experimental investigations, Proceedings of the 6th International Conference on Thin-Walled Structures Timisoara, Romania, Volume 2, 795-805, 2011, ISBN (ECCS): 978-92-9147-97-101.
[26] ABAQUS, Theory manual, Hibbit, Karlson and Sorenson Inc., 2007.
[27] EN1993-1-3. Eurocode 3: Design of steel structures – Part 1-3: General rules – Supplementary rules for cold-formed members and sheeting. Published by European Committee for Standardization, Brussels, 2006.
[28] Beque J. The interaction of local and overall buckling of cold-formed stainless steel columns, PhD. Thesis, The University of Sydney, School of Engineering, 2008.
[29] Schafer BW, Peköz T. Computational modelling of cold-formed steel: characterizing geometric imperfections and residual stresses. Journal of Constructional Steel Research, 47(3), 193–210, 1998.
[30] Gardner L, Nethercot DA. Behaviour of cold-formed stainless steel cross-sections, Proceedings of 9th Nordic Steel Construction Conference, Helsinki, Finland, 781-789, 2001.
[31] AS4100-1990: Australian Standard: Steel Structures, Homebush, Australia.
[32] Crisan A, Ungureanu V, Dubina D. Behaviour of thin-walled cold-formed steel perforated sections in compression. Part 2 – Numerical investigations, Proceedings of the 6th International Conference on Thin-Walled Structures

Timisoara, Romania, Volume 2, 805-813, 2011, ISBN (ECCS): 978-92-9147-102-107.
[33] Koen D. Structural capacity of light gauge steel storage rack uprights, Thesis presented for the degree of Master of Engineering, School of Civil Engineering, The University of Sydney, 2008.
[34] Gioncu V. General theory of coupled instability, thin-walled structures, Special Issue on Coupled Instability in Metal Structures (Rondal J, Gioncu V, Dubina D, Eds.), 19(2-4), 81-128, 1994.
[35] EN1993-1-1. Eurocode 3: Design of steel structures – Part 1-1: General rules and rules for buildings. Published by European Committee for Standardization, Brussels, 2005.